PAPER • OPEN ACCESS

Two years' test of a temperature sensing system based on fibre Bragg grating technology for the CMS GE1/1 detectors

View the article online for updates and enhancements.

Two years' test of a temperature sensing system based on fibre Bragg grating technology for the CMS GE1/1 detectors

M. Abbas[l], M. Abbrescia[r], H. Abdalla[i], S. Abu Zeid[i], A. Agapitos[e], A. Ahmad[aa], A. Ahmed[i], A. Ahmed[o], W. Ahmed[aa], S. Amarjeet[n], I. Asghar[aa], P. Aspell[ae], C. Avila[g], J. Babbar[n], Y. Ban[e], R. Band[ag], S. Bansal[n], L. Benussi[t], V. Bhatnagar[n], M. Bianco[ae], S. Bianco[t], K. Black[aj], L. Borgonovi[s], O. Bouhali[ab], A. Braghieri[v], S. Braibant[s], S. Butalla[ak], S. Calzaferri[v], M. Caponero[t*], F. Cassese[u], N. Cavallo[u], S. Chauhan[n], S. Colafranceschi[ak], A. Colaleo[r], A. Conde Garcia[ae], M. Dalchenko[af], A. De Iorio[u], G. De Lentdecker[a], D. Dell Olio[r], G. De Robertis[r], W. Dharmaratna[ad], S. Dildick[af], B. Dorney[a], R. Erbacher[ag], F. Fabozzi[u], F. Fallavollita[ae], D. Fiorina[v], E. Fontanesi[s], M. Franco[r], C. Galloni[aj], P. Giacomelli[s], J. Gilmore[af], M. Gola[o], M. Gruchala[ae], A. Gutierrez[ah], R. Hadjiiska[c], T. Hakkarainen[j], J. Hauser[ai], K. Hoepfner[k], M. Hohlmann[ak], H. Hoorani[aa], T. Huang[af], P. Iaydjiev[c], A. Irshad[aa], A. Iorio[u], J. Jaramillo[h], D. Jeong[y], V. Jha[q], A. Juodagalvis[z], E. Juska[af], T. Kamon[af], P. Karchin[ah], A. Kaur[n], H. Kaur[n], H. Keller[k], H. Kim[af], J. Kim[x], A. Kumar[o], S. Kumar[n], H. Kumawat[q], N. Lacalamita[r], J. Lee[y], A. Levin[e], Q. Li[e], F. Licciulli[r], L. Lista[u], F. Loddo[r], M. Lohan[n], M. Luhach[n], M. Maggi[r], N. Majumdar[p], K. Malagalage[ac], S. Malhorta[ab], S. Martiradonna[r], N. Mccoll[ai], C. McLean[ag], J. Merlin[r], D. Mishra[q], G. Mocellin[k], L. Moureaux[a], A. Muhammad[aa], S. Muhammad[aa], S. Mukhopadhyay[p], M. Naimuddin[o], P. Netrakanti[q], S. Nuzzo[r], R. Oliveira[ae], L. Pant[q], P. Paolucci[u], I. Park[y], L. Passamonti[t], G. Passeggio[u], A. Peck[ai], L. Petre[a], H. Petrow[j], D. Piccolo[t], D. Pierluigi[t], G. Raffone[t], M. Rahmani[ak], F. Ramirez[h], A. Ranieri[r], G. Rashevski[c], M. Ressegotti[v], C. Riccardi[v], M. Rodozov[c], C. Roskas[b], B. Rossi[u], P. Rout[p], J. D. Ruiz[h], A. Russo[t], A. Safonov[af], D. Saltzberg[ai], G. Saviano[t], A. Shah[o], A. Sharma[ae], R. Sharma[o], M. Shopova[c], F. Simone[r], J. Singh[n], E. Soldani[t], U. Sonnadara[ac], E. Starling[a], B. Stone[ai], J. Sturdy[ah], G. Sultanov[c], Z. Szillasi[m], D. Teague[aj], D. Teyssier[m], T. Tuuva[j], M. Tytgat[b], I. Vai[v], N. Vanegas[h], R. Venditti[r], P. Verwilligen[r], W. Vetens[aj], A. Virdi[n], P. Vitulo[v], A. Wajid[aa], D. Wang[e], K. Wang[e], N. Wickramage[ad], Y. Yang[a], U. Yang[x], J. Yongho[w], I. Yoon[x], Z. You[f], I. Yu[w], S. Zaleski[k]

on behalf of the CMS Muon Group

[a]Université Libre de Bruxelles, Bruxelles, Belgium
[b]Ghent University, Ghent, Belgium
[c]Institute for Nuclear Research and Nuclear Energy, Sofia, Bulgaria
[d]University of Sofia, Sofia, Bulgaria
[e]Peking University, Beijing, China
[f]Sun Yat-Sen University, Guangzhou, China
[g]University de Los Andes, Bogota, Colombia
[h]Universidad de Antioquia, Medellin, Colombia
[i]Academy of Scientific Research and Technology - ENHEP, Cairo, Egypt
[j]Lappeenranta University of Technology, Lappeenranta, Finland
[k]RWTH Aachen University, III. Physikalisches Institut A, Aachen, Germany
[l]Karlsruhe Institute of Technology, Karlsruhe, Germany
[m]Institute for Nuclear Research ATOMKI, Debrecen, Hungary
[n]Panjab University, Chandigarh, India
[o]Delhi University, Delhi, India
[p]Saha Institute of Nuclear Physics, Kolkata, India
[q]Bhabha Atomic Research Centre, Mumbai, India
[r]Politecnico di Bari, Università di Bari and INFN Sezione di Bari, Bari, Italy
[s]Università di Bologna and INFN Sezione di Bologna , Bologna, Italy
[t]Laboratori Nazionali di Frascati INFN, Frascati, Italy
[u]Università di Napoli and INFN Sezione di Napoli, Napoli, Italy
[v]Università di Pavia and INFN Sezione di Pavia, Pavia, Italy
[w]Korea University, Seoul, Korea
[x]Seoul National University, Seoul, Korea
[y]University of Seoul, Seoul, Korea
[z]Vilnius University, Vilnius, Lithuania
[aa]National Center for Physics, Islamabad, Pakistan
[ab]Texas A&M University at Qatar, Doha, Qatar
[ac]University of Colombo, Colombo, Sri Lanka
[ad]University of Ruhuna, Matara, Sri Lanka
[ae]CERN, Geneva, Switzerland
[af]Texas A&M University, College Station, USA
[ag]University of California, Davis, Davis, USA
[ah]Wayne State University, Detroit, USA
[ai]University of California, Los Angeles, USA
[aj]University of Wisconsin, Madison, USA
[ak]Florida Institute of Technology, Melbourne, USA
[*]Author to whom any correspondence should be addressed, michele.caponero@enea.it

Abstract. A temperature monitoring system based on fibre Bragg grating (FBG) fibre optic sensors has been developed for the gas electron multiplier (GEM) chambers of the Compact Muon Solenoid (CMS) detector. The monitoring system was tested in prototype chambers undergoing a general test of the various technological solutions adopted for their construction. The test lasted about two years and was conducted with the chambers being installed in the CMS detector and operated during regular experimental running. In this paper, we present test results that address the choice of materials and procedures for the production and installation of the FBG temperature monitoring system in the final GEM chambers.

1.   Introduction

Gas electron multiplier (GEM) chambers will be available in the endcaps of the Compact Muon Solenoid (CMS) detector for future experimental running starting in 2021, when the CERN Large Hadron Collider is expected to provide higher luminosity beams. A set of GEM chambers, referred to as GE1/1 chambers [1], is in an advanced production stage and will be the first to be operated.

In January 2017, several prototypes of the GE1/1 chambers were installed in the CMS detector and operated to test the adopted technology during regular experimental running [2]. The test activity, referred to as the GE1/1 Slice Test, lasted until the end of 2018. Among the technologies adopted to test the GE1/1 chambers, the fibre Bragg grating (FBG) technology was adopted to monitor their operating temperature, which is a critical parameter to have them working with best efficiency. FBG technology has a long history of use in CMS for temperature and structural monitoring of detector parts during regular running [3, 4]. FBG technology was also adopted in CMS during the early engineering development of the GEM chambers [5] and was eventually chosen for temperature monitoring of the chambers during regular running.

The interest of CMS in FBG technology is motivated by two of its peculiar features, both deriving from the spectroscopic character of the FBG sensor signal: immunity to electromagnetic disturbances and in-series cabling of multiple sensors. The former enables reliable monitoring in case of instability and during ramp-up/down of the magnetic field (a large part of the CMS detector is in a high magnetic field of up to 4 T). The latter permits simple cabling by using a single optical fibre to read out dozens of sensors by wavelength division multiplexing (in CMS, as in most high energy physics experiments, routing of cables is a critical issue faced by integration management).

For the Slice Test, two chambers were equipped with multi-point fibre-optic temperature-sensing systems based on FBG technology. FBG sensors were installed to monitor the temperature at six selected locations on the GE1/1 chamber structure, close to the electronic boards that perform local voltage control and signal preprocessing. These electronic boards are heat sources and are cooled by copper pads, which are part of a pumped-water refrigeration coil system. The FBG sensors monitor the temperature distribution of the active detector volume, which should be homogeneous and in a prefixed range for efficient operation of the chamber. The intent of the work presented in this paper was to test in regular running the materials and technical solutions adopted to equip the chambers with FBG sensors and to assess the efficiency of the pumped-water cooling system in maintaining the correct temperature distribution over the full detector surface.

This paper reports the results of continuous monitoring during the Slice Test running. We provide evidence of the effectiveness and reliability of the adopted FBG system, which shows that it is eligible for real-time and early-warning monitoring. Results collected during the Slice Test confirmed the efficiency of the cooling system and addressed the final choice of materials and procedures for the production of the FBG temperature monitoring system. Because the cooling system efficiently kept the temperature homogeneity within the required limits, in the final GE1/1 design only one FBG sensor per chamber will be used. The FBG system will provide real time control of the operating temperature with early warning of anomalous temperature variation, thus enabling the GEM chambers to work with best efficiency.

2.   Fibre Bragg grating sensors

Here we briefly recall that FBG sensors are fibre optical sensors, made by a modulation of the refraction index along a short segment of the fibre [6]. That modulation produces a phase diffraction Bragg grating, which acts as a wavelength-selective back reflector. If broadband radiation propagates along the fibre, at the interaction with the grating, a narrow band of radiation centred at the Bragg wavelength λ_B is reflected back along the fibre itself. Both temperature change ΔT and mechanical strain ε influence λ_B. The resulting variation $\Delta\lambda_{TOT}$ of λ_B can be expressed in the form

$$\Delta\lambda_{TOT} = \Delta\lambda_{TEMP} + \Delta\lambda_{STRAIN} = b \blacktriangledown \Delta T + a \blacktriangledown \varepsilon,$$

which shows how variation of the FBG signal encodes the values of the variation of strain and temperature. Typical values of b and a are about 1.0 picometre/K and about 1.2 picometre/microstrain, respectively. Spectroscopic analysis of the back-reflected wavelength λ_B is used to measure $\Delta\lambda_{TOT}$ and hence the values of the temperature change ΔT and mechanical strain ε occurring at the grating location.

FBG sensors can thus be used as temperature sensors and/or strain sensors, provided they are put in thermal and/or structural contact with the component to be monitored. The sensitivity to both temperature and strain is in general a positive feature, but it can become a drawback if the two measurands need to be disentangled. Disentangling is usually done by the use of two close FBG sensors, with one being in structural and thermal adherence (typically by gluing) and the other being in thermal contact only (typically by applying thermal grease/oil). Different and more complex disentangling techniques can be used, but they are usually reserved for cases with particular requirements, such as measuring disturbances due to temperature/strain shock excitation.

The spectroscopic nature of the FBG signal is the origin of many of the following useful features of the technology. 1) Easy cabling, with many sensors connected in series and operated by wavelength division multiplexing: the full bandwidth of the light launched into the fibre is ideally divided into sub-bandwidths and each sensor of the chain operates in one of them. 2) Immunity to electromagnetic disturbances: the spectroscopic signal can only be affected by an appreciable variation of the magnetic permeability of the optical fibre, which cannot be caused even by the highest magnetic fields. 3) Long term stability: the technology for producing very stable reference wavelengths is at hand; instruments have built-in modules for permanent calibration and thermal-drift compensation. 4) Durability and robustness to environment disturbances: ageing of components, loosening of connectors, vibrations, etc., can affect the signal amplitude but cannot affect the signal spectrum. 5) Radiation hardness: exposure to ionizing radiation increases the fibre transmission loss and hence increases the signal attenuation, but does not affect the signal spectrum; a high radiation dose at the FBG sensors causes both drifting of the Bragg wavelength and lowering of the Bragg diffraction, but its radiation hardness is adequate for most nuclear and high energy physics experiments.

3.   The GE1/1 chambers

Figure 1 (left) shows a conceptual sketch of an exploded GE1/1 chamber. The active volume is a drift chamber with three GEM foils between the bottom and top walls. The top wall, called the reading board (RB), is a double-layer printed circuit board: the channels of the chamber are printed on the inner surface and are terminated in sockets on the outer surface. The three GEM foils are held in place by the inner frame, stretched parallel with a thin gap between each foil. The bottom wall is kept polarised to cause drifting of the charges toward the RB with avalanche production while passing through holes in the GEM foils. The outer frame serves as the lateral walls of the chamber and provides the required mechanical stiffness. A printed circuit board called the GEM electronic board (GEB) hosts the on-board readout electronics and is equipped with sockets for bridge connections with the sockets of the RB. A copper pipe with pads in thermal contact with the on-board electronic components provides the necessary cooling of the GE1/1 chamber. Aluminium shielding on top of the full assembly provides a smooth top surface and some mechanical protection.
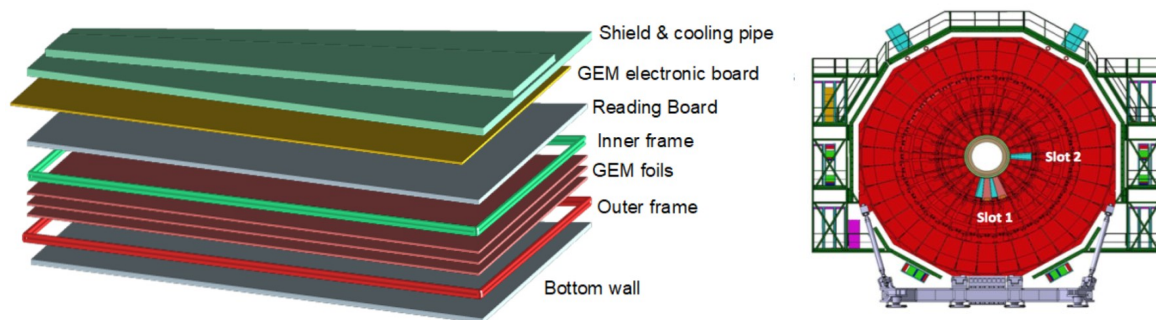
Figure 1. Left: exploded diagram of a GE1/1 chamber with the main component parts and their naming identified. Right: sketch of the CMS detector disk where the GE1/1 chambers will be installed, showing the position of the prototype superchambers installed for the GE1/1 Slice Test.

Because of constraints from the general design of the CMS detector, there are two different types of GE1/1 chambers. The difference being primarily in the length, they are referred to as long and short chambers. GE1/1 chambers are assembled in pairs of the same type (either both long or both short) and the assembled pair is referred to as a superchamber. Part of the CMS detector is a stack of disks with a central hole: each disk is divided in concentric rings; each ring is made of detectors with trapezoidal planar surface. Figure 1 (right) shows the disk on which the GE1/1 superchambers will be installed; the concentric rings made of detectors with trapezoidal surface can be seen. The GE1/1 detectors will be assembled as a ring made of 18 long superchambers and 18 short superchambers, with the two types alternating along the ring. A few prototype GE1/1 chambers were used to test the technologies adopted for their construction. The Slice Test was conducted during regular experimental running from January 2017 until the end of 2018. The prototype chambers were assembled as superchambers and installed in the CMS detector. Figure 1 (right) shows the locations selected for the GE1/1 Slice Test in the CMS detector (5/36 of the full ring: one short superchamber in Slot 2 and two long and two short superchambers in Slot 1).

4.   Installation of the FBG sensors

FBG sensors were installed on the two GE1/1 short chambers (called L01 and L02) assembled as the short superchamber placed in Slot 2 (Fig. 1). The temperature monitoring system is composed of six FBG sensors positioned at selected locations on the RB; the FBG sensors are thus all between the RB and the GEB. The specific locations of the six FBG sensors on the RB were chosen to monitor the temperature distribution with consideration of the locations of the electronic boards installed on the GEB, which behave as local heat sources. Figure 2 (left) shows the positions of the six FBG sensors on the RB. Also shown is the routing of the fibre along which the six sensors are connected in series, as a chain. Figure 2 (right) shows a sensor chain after its production, coiled on a storage tray prior to installation.

Cabling of the sensors in the form of a chain of sensors along a single optical fibre is possible because each sensor operates at a different nominal wavelength. Data can thus be collected by wavelength division multiplexing, the signal of each sensor staying within a different wavelength band. Figure 3 shows the six FBG sensors laid down on the RB of a prototype chamber. The FBG sensors are circled and the nominal working wavelength of each sensor is shown. On the right, the two ends of the chain can be seen plugged into the green adapter mounted on the patch panel of the chamber. FBG sensors sense heating of the RB, which in turn heats the underlying active gas volume (i.e., the gas volume in which the GEB foils are stretched). FBG sensors thus provide early warning of the occurrence of transitory events that can affect the temperature of the active volume. FBG sensors can be assumed to monitor the temperature of the active volume of the chamber, provided that long/medium-term steady conditions apply.
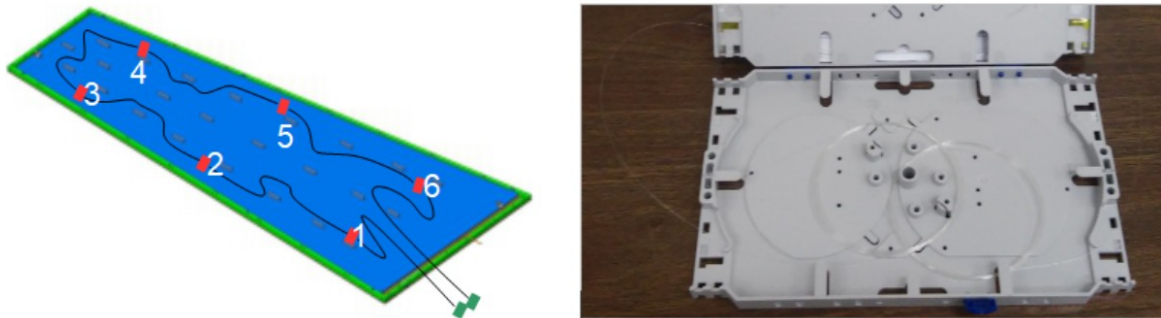
Figure 2. Left: sketch of the reading board (RB), showing the position of the six FBG sensors and the cable routing. Right: a chain of sensors coiled on a storage tray prior to installation.

The sensor chains were custom produced using commercial FBG sensors. After trimming their pigtails for correct spacing along the chain, they were connected in series by fusion splicing and acrylate recoating. The commercial FBG sensors (T&S Communications Co. Ltd., China) are 10 mm long. They were produced with bare acrylate-coated optical fibre (outer diameter = 0.25 mm) with a 1 m long pigtail on both sides. Fibre optic connectors (LC/APC type) attached to both ends of the chain are plugged into adapters mounted on the chamber patch panel. In its final state, the chain's optical fibre is bare, with no use of protective tubing apart from a small segment close to the optical connector at the two ends for protection while handling the connectors and for plugging them into and out of the adapters. The outer diameter of the tubing at the connectors is 0.90 mm with a length of 15 mm.
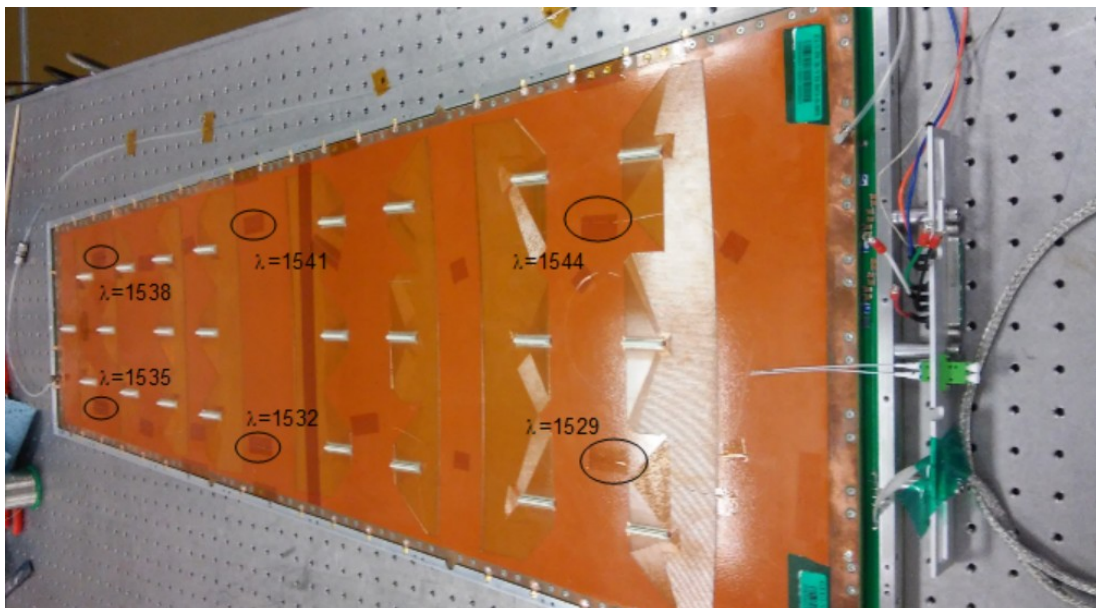

Figure 3. The six FBG sensors (circled), installed on the RB of a prototype chamber.

With an outer diameter of 0.25 mm, the chain can stay securely between the RB and the GEB, being most part of their surfaces thinly spaced or in very loose contact. In fact the GEB is not laid on the RB but it is fixed along its perimeter at the outer frame, thus the sensor chain is not subject to unsafe compression. Each FBG sensor stays in direct contact with the RB, held in place and slightly stretched by Kapton® adhesive tape. After installation, FBG sensors have both thermal and structural adherence to the RB. In general, structural and thermal disturbance can not be disentangled by use of one FBG sensor, but in our application no direct (i.e. due to external forces) mechanical disturbances of the RB is expected after the chamber is fully assembled and is being operated. Thus, pure thermal sensing can be assumed although with some part of the disturbance being due to the thermally induced

structural deformation of the monitored surface. The absence of direct mechanical disturbances at the FBG sensors was confirmed experimentally: no appreciable disturbance was measured by any sensor, neither while the chambers were handled in a simulation of the foreseen installation procedure, nor while the chambers were loaded in a simulation of the final constrained condition. Temperature sensing calibration of the FBG sensors was done after the chambers were fully assembled.

5.   The Slice Test run

Figure 4 shows the time history of data from the L02 chamber during the period April–September 2018. The top plot shows the temperature change monitored by three FBG sensors. The bottom plot shows the current absorbed on one power supply line by the electronic boards. Correlation of the temperature change with the current absorbed by the electronic boards can be easily seen in Fig. 4, despite the compressed time scale. The same result holds in any period, for any sensor, for both the L02 and L01 chambers.
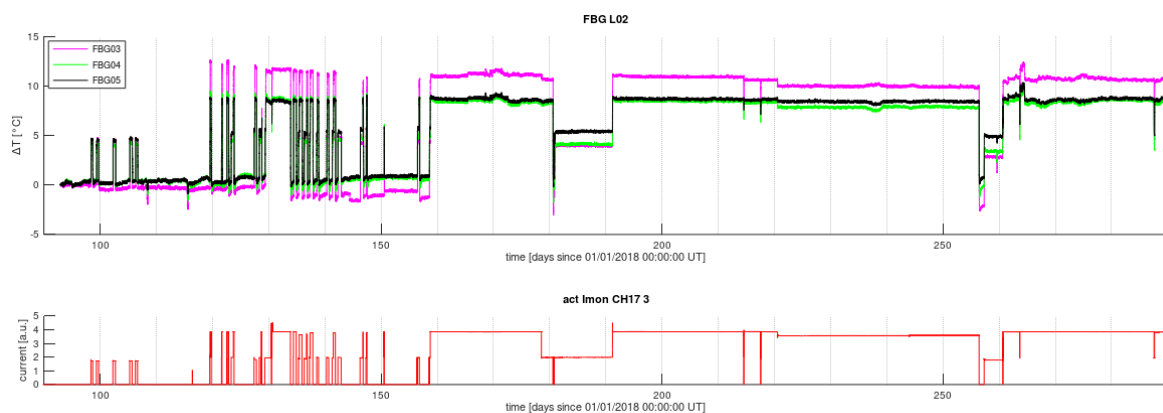
Figure 4. Top: time history of FBG temperature change data for L02. FBG sensors are named as in Fig. 2. Data from only three out of the six sensors are shown to make the graph clearer. Bottom: time history of the absorbed current.

Data from a different monitoring time interval and from all the sensors are shown in Fig. 5 for deeper insight. The top graph shows L01 temperature change data from the six FBG sensors. The bottom graph shows the current absorbed by the electronic boards on all their power supply lines. The short time history from 12 September to 14 October 2017 represents a time scale that can be adequately expanded to show visual evidence of the variation of the two graphs over time. However, it is fully representative of the results from the full test, which ran from the beginning of 2017 until the end of 2018. A strong correlation between the temperature change and the current absorbed by the electronic boards is evident: an increase (decrease) of the absorbed current always triggers heating toward a higher (lower) steady temperature.

Heating and cooling events not correlated with the absorbed current are correlated with activities concerning various issues reported in the CMS logbook that mostly concern the maintenance and regulation of the cooling system. In Fig. 5, some heating not related to the absorbed current or to cooling maintenance can be seen around day 127.5 (the start of the event is marked by the red vertical line). The CMS experiment's e-logbook reports that activities were performed to test the controller/driver of the electronic boards, evidently affecting their condition, for about 1 h before the chambers were turned on around day 127.6, when a heating event clearly correlated with the increase of the adsorbed current can be seen.
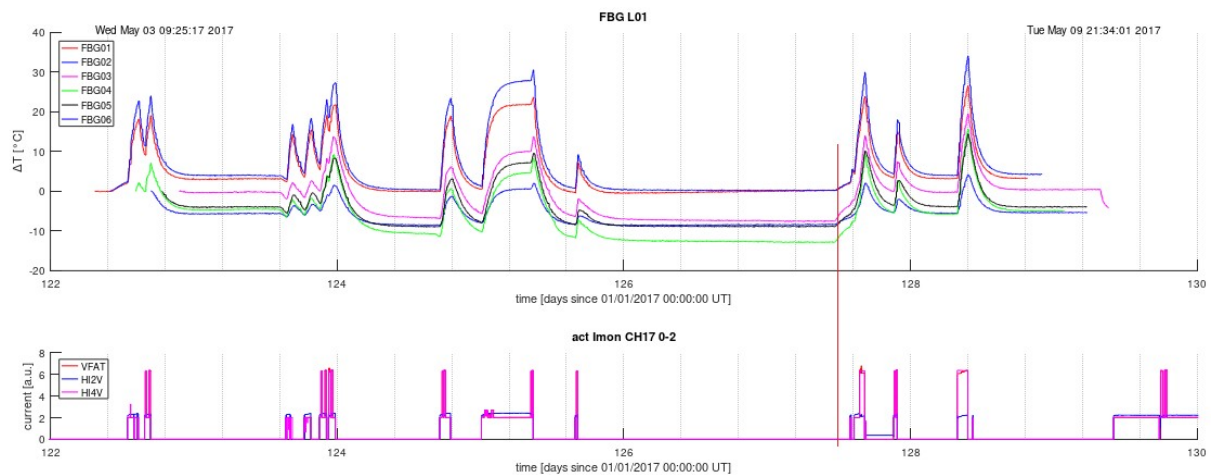
Figure 5. Same as Fig. 4, but for all six L01 sensors and a different time interval.

As an example, Fig. 6 shows a maintenance intervention event. The time history shows that a temperature increase occurred while the flux of the coolant was stopped for about 7 h to fix a leak. The time history also shows that no current was absorbed by the electronic boards (obviously, chambers were switched off during the intervention), indicating that the heating that occurred is related only to the temporary lack of cooling.
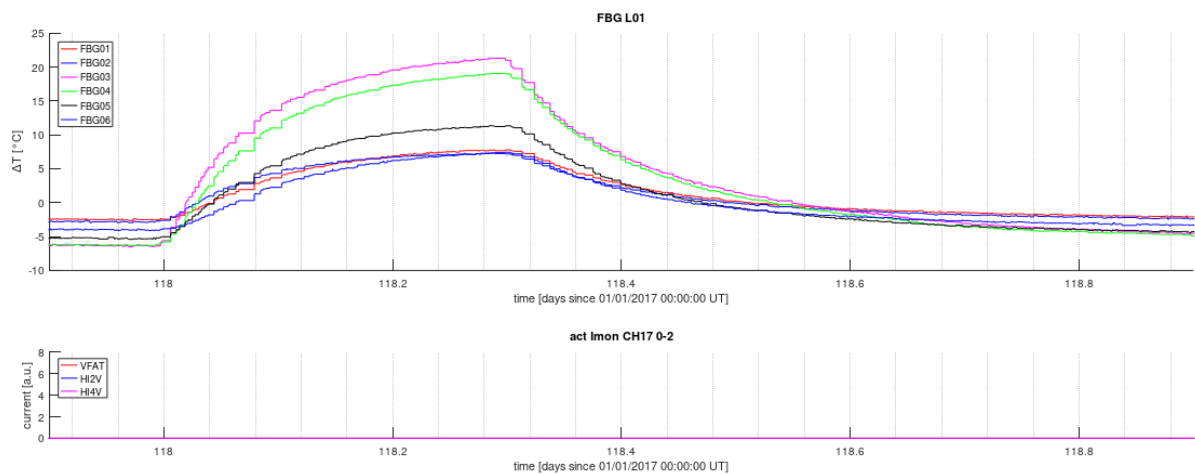
Figure 6. Time history of (top) FBG sensors and (bottom) absorbed current when the coolant flux was stopped for a maintenance intervention.

Figure 7 shows events occurring before, during, and after a ramp-up of the CMS magnetic field to 3.8 T. As expected, the graphs confirm the absence of any effect on the FBG sensors by the different regimes of the magnetic field and the services of the magnet. In fact, along the full time history, all FBG sensors provided signals clearly correlated with the current absorbed by the electronic boards, with no evidence of any correlation with the ramping/stepping of the magnetic field.
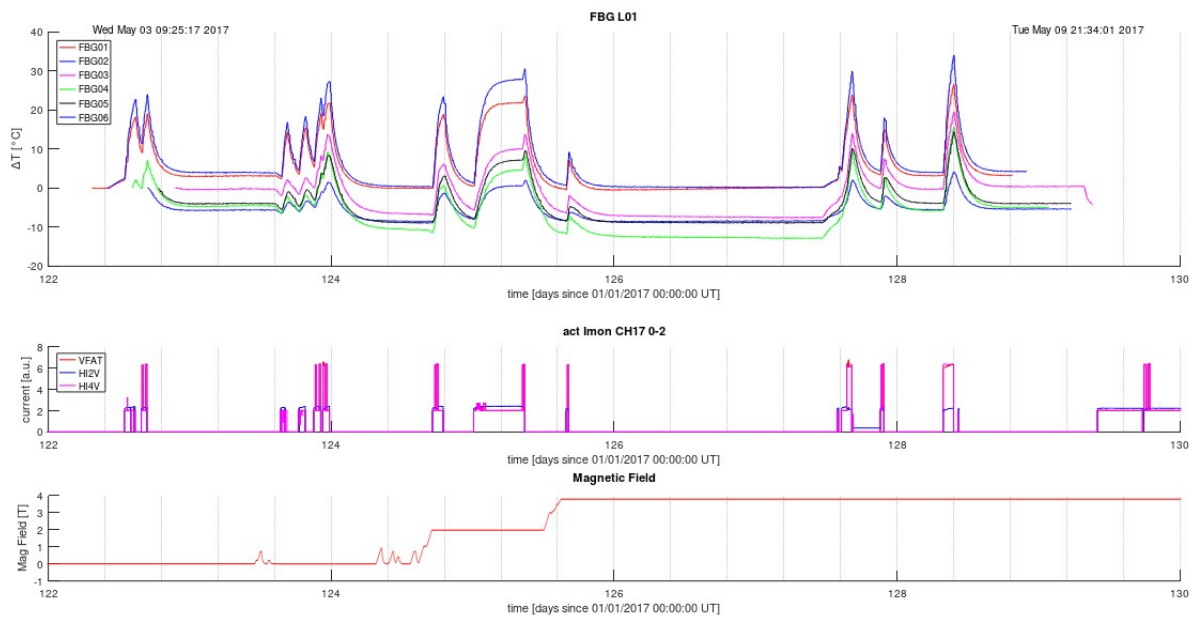
Figure 7. Time history of (top) FBG sensors, (middle) absorbed current, and (bottom) magnetic field for L01.

6.   Conclusions

The use of FBG sensors for temperature monitoring in the CMS GE1/1 detectors was successfully tested during long-term regular experimental running. The adopted materials and the technique to install the sensors between the GEB and the RB were shown to be adequately robust for any condition that occurred during regular running. The FBG monitoring system was found to be well suited not to sense purely mechanical disturbances of the chambers. In fact, all events recorded by the FBG sensors were correlated with actions that should be expected to affect the temperature of the chambers and allowed for better evaluation of their effects. Results from the Slice Test addressed the production of the FBG temperature monitoring system installed in the final GE1/1 detectors and will contribute to the final designs of the FBG temperature monitoring systems planned for the other sets of GEM chambers that will be installed in CMS, namely GE2/2 and ME0.

References

[1]   CMS Collaboration 2015 CMS Technical Design Report for the Muon Endcap GEM Upgrade *CERN-LHCC-2015-012, CMS-TDR-013.*
[2]   Vai I 2019 *Nuclear Instruments and Methods in Physics Research Section A: Accelerators, Spectrometers, Detectors and Associated Equipment* **936** 439–41.
[3]   Buontempo S, Breglio G, Consales M, Cusano A, Fienga F, Gaddi A, Shaefer C, Beni N, and Szillasi Z 2017 SHM in CMS underground detector at CERN using FBG sensors *Proc. 11th International Workshop on Structural Health Monitoring, IWSHM 2017 (Stanford University).*
[4]   Berruti G, Petagna P, Buontempo S, Makovec A, Szillasi Z, Beni N, Consales M, and Cusano Andrea 2016 *Journal of Instrumentation* **11** P03007
[5]   Abbaneo D *et al.* 2018 *EPJ Web Conf.* **174** 03002
[6]   Hill K and Meltz G 1997 *Journal of Lightwave Technology* **15** 1263–76